ACS OMEGA

Open Access

http://pubs.acs.org/journal/acsodf

Article

Semianalytical Modeling for Multiphase Flow in a Fractured Low-Permeability Gas Condensate Reservoir

Fuguo Yin,* Shiqing Cheng, Xiuwei Liu, Lijun Zhang, Huisheng Liu, Wenpeng Bai, DengKe Shi, and Yang Wang

Cite This: *ACS Omega* 2023, 8, 32892−32906

Read Online

ACCESS | Metrics & More | Article Recommendations

ABSTRACT: During the production of fractured low-permeability gas condensate reservoir (FLPGCR), a phase transition takes place in both the formation and wellbore, resulting in multiphase flow when the pressure drops below the dew point pressure. Additionally, the presence of fractures causes the formation of stress-sensitive characteristics. Nevertheless, traditional analytical models, such as the two-region model or three-region model, overlook the coupling impact of the above factors, which could lead to incorrect pressure transient response and erroneous estimation of well and formation parameters. Therefore, this work presents a semianalytical model for an FLPGCR considering the effects of multiphase flow, stress-sensitive, and wellbore phase redistribution. The gas condensate reservoir is divided into N banks, and the radial fluid saturation variation is modeled by multiple annular reservoirs with a constant saturation in each annular reservoir. The behavior of a fractured reservoir is modeled by using the dual-porosity model. The Pedrosa transform was utilized to address the nonlinear differential equation arising from stress-sensitive behavior. To verify the semianalytical solution, it was compared with numerical simulation results from CMG. The results showed that there are 10 flow regimes for the proposed model. The shape of the type curve has the potential to identify the degree of blockage within the FLPGCR. The wellbore phase redistribution only affects the first transitional-flow regime, which slows the rate of pressure drop. The stress sensitivity will lead to the upward characteristic of the curve in a later stage. More attention should be paid to the upward pressure derivative curve at late times, which is conventionally regarded as the effect of a closed boundary when it may not be the case. In addition, the shape factor and composite radius may obscure the radial flow regime. Finally, the proposed model was applied to interpret the pressure measurements recorded from the Bohai field in China, which exhibits a better fitting quality than the traditional models.

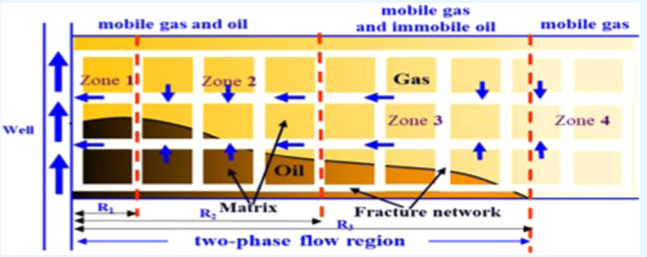

1. INTRODUCTION

In recent years, due to the depletion of many conventional hydrocarbon reservoirs in the world, the tendency to develop unconventional reservoirs is dramatically increasing, including gas condensate, shale gas, and tight gas.[1] According to statistics, in the geological reserves of more than 1×10^{12} m^3 of giant gas fields, the condensate field accounts for 68%. As illustrated in Figure 1, gas condensate reservoirs exhibit intricate flow dynamics when the pressure drops below the dew point pressure. The decrease in pressure induces retrograde condensation, resulting in the formation of a condensate bank within the gas reservoir. With pressure decreasing, more condensation drops out and the saturation of the condensate reaches the critical level.[2] This leads to not only the free flow of gas but also the flow of condensate within the formation. If the condensate flow is not taken into consideration, there will be significant errors in pressure transient analysis.[3,4] The phenomenon of wellbore phase redistribution also occurs in the production of the gas condensate reservoir which shows the changeable wellbore storage characteristic observed in transient pressure analysis.[5,6] The existence of natural fractures is another difficult problem in gas condensate reservoir development, which not only impacts the flow behavior of fluids but also induces a stress-sensitive effect in the formation.[7] The gas condensate reservoir in the Bohai field is a fractured low-permeability condensate gas reservoir. Its pressure transient analysis curve exhibits a complex shape that is difficult to interpret by the existing models. Therefore, analyzing the abnormal curve of a gas condensate reservoir could be challenging in well-testing interpretation.

Received: June 18, 2023
Accepted: August 21, 2023
Published: August 31, 2023

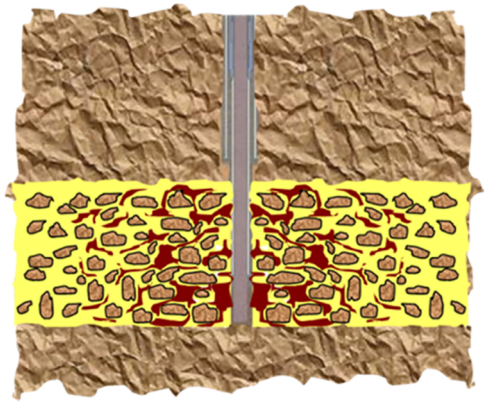

Figure 1. Condensate fluids occur as the pressure drops below the dew point pressure.

It is difficult to explain the pressure characteristics of FLPGCR because of the complex fluid flow in formation caused by multiphase flow and natural fractures. In order to solve this problem, a lot of research has been done. Muskat described the "condensate blockage" for the first time in their study: when the bottom-hole pressure (BHP) falls below the dew point pressure, condensate will be formed near the bottom of the well and gradually accumulate to form the high saturation area of condensate, which will lead to the decrease of gas-phase relative permeability and the decrease of production capacity.[8] The concept of pseudopressure was originally proposed by O'Dell and Miller, who subsequently applied it to the productivity formula of gas condensate reservoirs.[9] Jones proposed the concept of multiphase pseudopressure for gas condensate reservoirs.[10] Subsequently, various pressure transient analysis models utilizing the concept of pseudopressure have been developed, ushering in a new era of research in pressure transient analysis for gas condensate reservoirs. Jones and Rgahvana studied the steady-state model of gas condensate reservoirs and established a relationship between oil saturation and pressure.[11] Their findings indicated the presence of a condensate oil flow region in the reservoir with a condensate saturation exceeding the critical condensate saturation. Fevang and Whitson conducted a study on the production behavior of gas condensate reservoirs using numerical simulation and introduced a mathematical model for three-zone flow for the first time.[12] Later, Xu and Lee proposed the radial three-zone composite two-phase flow model.[13] Gringarten introduced the effect of the capillary number into numerical simulation and found that the condensate saturation near the well was not as high as commonly thought, but lower than in other areas.[14] Therefore, a four-zone model is proposed to describe condensate flow behaviors. Barrios used a compositional simulation model to analyze pressure transient responses in gas condensate reservoirs, including the effects of relative permeability effects and critical oil saturation effect.[15] Abdolnabi and Gringarten applied composite models to horizontal wells.[16,17] Bozorgzadeh and Kgogo each gave an opinion that the type curves of lean and medium-rich condensate gas fluids have three-zone radial composite behavior.[18,19] However, rich gas fluids exhibit only two-region radial composite behavior.[20] Shahbazi and Zhang proposed an analytical model to explain well test data in gas condensate reservoirs which provided a detailed explanation of the pressure transient analysis curve characteristics for horizontal wells.[21,22] Li presented a semianalytical model considering different gas components of the gas condensate reservoir.[23] Dastan proposed a semianalytical model for natural fractured reservoirs under the condition of oil−water two-phase flow.[24] This model is considered a multibank reservoir, which has great significance in solving multiphase flow models. Dahim proposed a semianalytical model for multistage hydraulically fracturing horizontal wells in shale gas condensate reservoirs, which is also of great significance in solving multiphase flow problems.[25] Among the analytical models considering the development of natural fractures, the dual-porosity model presented by Warren and Root and the vertical fractured model proposed by Aguilera were the most widely used.[26,27] The fluid flow in fractured reservoirs has always been a focal point and a challenge in the field of petroleum engineering. In recent studies, Wang proposed a semianalytical model to describe the bottom-hole pressure behavior of water injectors in fractured reservoirs.[28,29] Wei developed analytical models to study the thermal behavior of fractured reservoirs. These studies provide novel approaches to address the fluid flow challenges in fractured oil reservoirs, aiding in the solution of the nonlinear flow equations of FLPGCR.[30]

In summary, many researchers have studied the pressure transient analysis of multiphase flow in the gas condensate reservoir. However, much less attention has been paid to the analysis of the multiphase flow combined effects specifically related to natural fractures and wellbore phase redistribution. Neglecting the interconnected influences of these factors could lead to inaccurate pressure transient analysis and erroneous

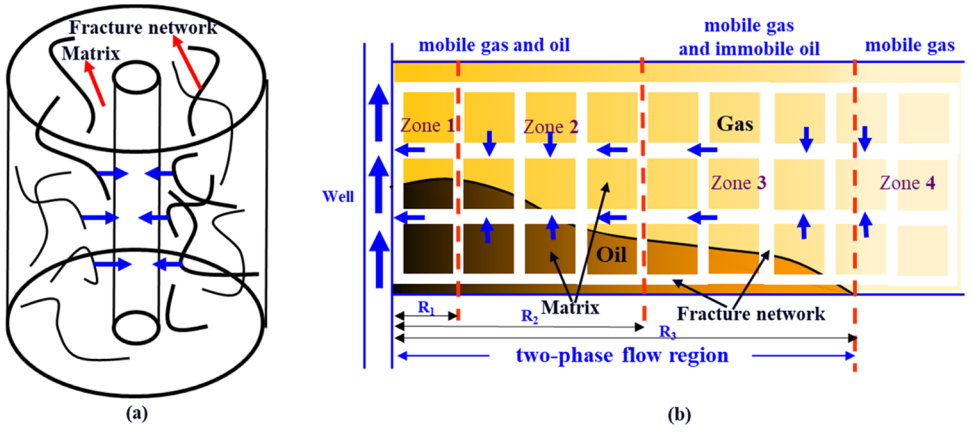

Figure 2. Physical model of FLPGCR based on the Warren−Root dual-porosity model: (a) Actual model of FLPGCR and (b) ideal model.

https://doi.org/10.1021/acsomega.3c04183
ACS Omega 2023, 8, 32892−32906

assessments of well and formation parameters in FLPGCR. In this study, a semianalytical model considering multiphase flow is developed to characterize flow behavior in FLPGCR. In order to analyze the occurrence of retrograde condensation, a four-region radial composite model was utilized, whereas the effects of natural fractures were simulated using the Warren and Root model. Additionally, the wellbore phase redistribution was described by implementing the Fair model. To account for the stress-sensitive impact, the variation of permeability in the fracture with pressure was taken into consideration. To solve the model, the whole reservoir is divided into a sequence of N banks, considering the saturation change. The semianalytical solution is verified by comparing it with a numerical simulation model from CMG.[31] The solutions derived from the model can be presented in the form of type curves, which effectively show the influence of retrograde condensation and natural fracture. Finally, the proposed model has been successfully applied to interpret a field case in the Bohai field.

2. METHODOLOGY

2.1. Physical Model. The flow behaviors of the gas condensate reservoir in the formation are much more complex. Laboratory experiments suggest that four different flowing regions could exist.[32] Figure 2 shows the physical model of FLPGCR, where four distinct flow zones with varying fluid saturations are present around the wellbore due to retrograde condensation.

The area near the well is a two-phase flow zone, where condensate saturation reaches critical levels. This area can be divided into two zones, including zone-1 and zone-2. Zone-1 is in the immediate vicinity of the wellbore with a lower condensate saturation due to the influence of the high capillary number.[33] Zone-2, which is next to zone-1, exhibits a higher level of condensate saturation compared to Zone-1. Zone-3 is an intermediate transition region, where the condensate is immobile. Zone-4 is a dry gas region, where retrograde condensation does not occur. The assumptions of the mathematical model are given as follows:

(a) The gas condensate reservoir is an infinite homogeneous double-porosity reservoir, which can be divided into four zones. The initial reservoir pressure p_i is higher than the dew point pressure and the reservoir thickness is h. The fracture is a stress sensitivity medium and the permeability modulus λ is introduced to characterize the stress sensitivity. The compressibility of fracture and matrix are c_{ft} and c_{mt}, respectively.
(b) There is no pressure drop at the interface of each region.
(c) The fluid is two-phase with viscosity μ_g and μ_o, compressibility c_g and c_o, and formation volume factor B_g and B_o.
(d) The flowing of fluid obeys Darcy's flow and is isothermal. The Warren−Root model is used to describe the fractures. The Fair model is used to describe the wellbore phase redistribution.

2.2. Analytical Model. The permeability of fractures is a function of the pressure rather than a constant. The relationship between the permeability and pressure is as follows

$$\gamma = \frac{1}{K_f}\frac{\partial K_f}{\partial p} \tag{1}$$

According to the Warren−Root model, the flow equation of oil and gas in fracture of Zone-1 can be expressed, respectively, as follows. The detailed derivation of eqs 2−7 is given in Appendix A.

$$\text{oil: } \frac{1}{r}\frac{\partial}{\partial r}\left[r\left(\frac{K_{1f}e^{-\gamma(p_i-p)}K_{rfo}}{\mu_o B_o}\right)\frac{\partial p}{\partial r}\right] = F_s\frac{K_{1m}K_{rmo}}{\mu_o B_o}(p_m - p_f) + S_{fo}\phi_f c_{fto}\frac{\partial p_f}{\partial t} \tag{2}$$

$$\text{gas: } \frac{1}{r}\frac{\partial}{\partial r}\left[rK_{1f}e^{-\gamma(p_i-p)}\left(\frac{K_{rfg}}{\mu_g B_g} + \frac{K_{rfo}}{\mu_o B_o}R_s\right)\frac{\partial p}{\partial r}\right] = F_s\left(\frac{K_{1m}K_{rmg}}{\mu_g B_g} + \frac{K_{1m}K_{rmo}}{\mu_o B_o}R_s\right)(p_m - p_f) + S_{fg}\phi_f c_{ftg}\frac{\partial p_f}{\partial t} \tag{3}$$

The flow equation in the matrix under pseudo-steady state of Zone-1 can be expressed as

$$\text{oil: } F_s\frac{K_{1m}K_{1mro}}{\mu_o}(p_m - p_f) + S_{mo}\phi_m c_{mto}\frac{\partial p_m}{\partial t} = 0 \tag{4}$$

$$\text{gas: } F_s\left(\frac{K_{1m}K_{mrg}}{\mu_g} + \frac{K_{1m}K_{mro}}{\mu_o}R_s\right)(p_m - p_f) + S_{mg}\phi_m c_{mtg}\frac{\partial p_m}{\partial t} = 0 \tag{5}$$

The total flow equation of Zone-1 between fracture and matrix can be expressed as

$$m_{1f}\frac{1}{r}\frac{\partial}{\partial r}\left[re^{-\gamma(p_i-p)}\frac{\partial p}{\partial r}\right] = m_{1m}F_s(p_m - p_f) + \phi_f c_{ft}\frac{\partial p_f}{\partial t} \tag{6}$$

$$F_s m_{1m}(p_m - p_f) + \phi_m c_{mt}\frac{\partial p_m}{\partial t} = 0 \tag{7}$$

In the multiphase model, compressibilities in the matrix and the fractures also depend on saturation:

$$c_{ft} = S_{fo}c_{fto} + S_{fg}c_{ftg} \tag{8}$$

$$c_{mt} = S_{mo}c_{mto} + S_{mg}c_{mtg} \tag{9}$$

The mobilities in Zone-1 and Zone-2 can be expressed as

$$\begin{cases} m_{if} = K_{if}\left(\dfrac{K_{rfo}}{\mu_o B_o} + \dfrac{K_{rfg}}{\mu_g B_g} + \dfrac{K_{rfo}}{\mu_o B_o}R_s\right) \\ m_{im} = K_{im}\left(\dfrac{K_{rmo}}{\mu_o B_o} + \dfrac{K_{rmg}}{\mu_g B_g} + \dfrac{K_{rmo}}{\mu_o B_o}R_s\right) \end{cases} i = 1, 2 \tag{10}$$

For Zone-3

$$\begin{cases} m_{3f} = K_{3f}\left(\dfrac{K_{rfg}}{\mu_g B_g}\right) \\ m_{3m} = K_{3m}\left(\dfrac{K_{rmg}}{\mu_g B_g}\right) \end{cases} \tag{11}$$

For Zone-4

https://doi.org/10.1021/acsomega.3c04183
ACS Omega 2023, 8, 32892−32906

Table 1. Dimensionless Variables and Their Definition

dimensionless variable	definition	dimensionless variable	definition
dimensionless fracture pressure	$p_D = \frac{2\pi kh}{qB}(p - p_i)$	dimensionless time	$t_D = \frac{tm_{f1}}{(\varphi_m c_{mt} + \varphi_f c_{ft}) r_w^2}$
dimensionless coordinates	$r_D = \frac{r}{r_w}$	dimensionless wellbore storage	$C_D = \frac{C}{2\pi(\phi c_t)_{f+m} h r_w^2}$
dimensionless mobility ratio	$M_i = \frac{m_{if}[c_{(i+1)ft} + (\rho_o - \rho_g)\partial S_o / \partial p]}{m_{(i+1)f}[c_{ift} + (\rho_o - \rho_g)\partial S_o / \partial p]}$ $i = 1, 2, 3$		

$$\begin{cases} m_{4f} = K_{rfg}(S_{gi})\left(\dfrac{1}{\mu_g B_g}\right) \\ m_{4m} = K_{rmg}(S_{gi})\left(\dfrac{1}{\mu_g B_g}\right) \end{cases} \tag{12}$$

Table 1 shows the definition of dimensionless variables

For a two-phase flowing problem in the Warren−Root model, we define interporosity flow coefficient (Λ) and two-phase storativity ratio (Ω) considering the mobility as given in eq 13 and eq 14

$$\Lambda_1 = \frac{F_s m_{1m} r_w^2}{m_{1f}} \tag{13}$$

$$\Omega = \frac{\varphi_f c_{ft}}{\varphi_f c_{ft} + \varphi_m c_{mt}} \tag{14}$$

In the Warren−Root model, F_s is a shape factor that depends on the fracture-matrix geometry. It can be calculated for structures with regular, repetitive geometries. Rangel−German and Kovscek tabulate different shape factors for a variety of geometries.[34] In practice, F_s can be taken as a fit parameter in the history matching. The dimensionless diffusivity equations of Zone-1, Zone-2, Zone-3, and Zone-4 in the FTCGR are obtained as follows

$$\begin{cases} \dfrac{1}{r_D}\dfrac{\partial}{\partial r_D}\left(r_D e^{-\gamma p_{fD}^{(i)}} \dfrac{\partial p_{fD}^{(i)}}{\partial r_D}\right) = (1 - \Omega)\dfrac{\partial p_{mD}^{(i)}}{\partial t_D} + M_i \Omega \dfrac{\partial p_{fD}^{(i)}}{\partial t_D} \\ (1 - \Omega)\dfrac{\partial p_{mD}^{(i)}}{\partial t_D} = -\Lambda_i (p_{mD}^{(i)} - p_{fD}^{(i)}) \end{cases}_i$$
$$= 1, 2, 3, 4 \tag{15}$$

The connection conditions are that the pressure and fluid rate of the common boundary are the same.

$$\begin{cases} p_{fD}^{(1)}(r_{D1}, t_D) = p_{fD}^{(2)}(r_{D1}, t_D) & \left.\dfrac{\partial p_{fD}^{(1)}}{\partial r_D}\right|_{r_D = r_{D1}} = \dfrac{1}{M_2}\left.\dfrac{\partial p_{fD}^{(2)}}{\partial r_D}\right|_{r_D = r_{D1}} \\ p_{fD}^{(2)}(r_{D2}, t_D) = p_{fD}^{(3)}(r_{D2}, t_D) & \left.\dfrac{\partial p_{fD}^{(2)}}{\partial r_D}\right|_{r_D = r_{D2}} = \dfrac{M_2}{M_3}\left.\dfrac{\partial p_{fD}^{(3)}}{\partial r_D}\right|_{rD = r_{D2}} \\ p_{fD}^{(3)}(r_{D3}, t_D) = p_{fD}^{(4)}(r_{D3}, t_D) & \left.\dfrac{\partial p_{fD}^{(3)}}{\partial r_D}\right|_{r_D = r_{D3}} = \dfrac{M_3}{M_4}\left.\dfrac{\partial p_{fD}^{(4)}}{\partial r_D}\right|_{rD = r_{D3}} \end{cases} \tag{16}$$

where $M_1 = 1$.

The outer boundary condition is as follows

$$p_{fD}^{(4)}(\infty, t_D) = p_{fD}^{(4)}(\infty, t_D) = 0 \tag{17}$$

The inner boundary condition considering wellbore phase redistribution is

$$\begin{cases} C_D\left(\dfrac{\partial p_{wD}}{\partial t_D} - \dfrac{\partial p_{\varphi D}}{\partial t_D}\right) - r_D e^{-\gamma p_{fD}^1}\left.\dfrac{\partial p_{fD}^{(1)}}{\partial r_D}\right|_{r_D = 1} = 1 \\ p_{wD} = \left(p_{fD}^{(1)} - S r_D e^{-\gamma p_{fD}^1}\left.\dfrac{\partial p_{fD}^{(1)}}{\partial r_D}\right|_{r_D = 1}\right) \end{cases} \tag{18}$$

The initial condition is given as

$$p_{fD}^{(i)}(r_D, 0) = p_{mD}^{(i)}(r_D, 0) = 0, \quad i = 1, 2, 3, 4 \tag{19}$$

The phase redistribution pressure is as follows[35]

$$p_{\varphi D} = C_{\varphi D}(1 - e^{-t_D/\alpha_D}) \tag{20}$$

The diffusivity equation is not written in a convenient form to be solved analytically. A new dimensionless dependent variable is introduced, which is related to the dimensionless pressure.[36]

$$p_D = -\frac{1}{\gamma_D}\ln(1 - \gamma_D \eta_D) \tag{21}$$

Making use of Pedrosa variable substitution, eq 21, the following partial differential equation can be obtained:

$$\begin{cases} \dfrac{1}{r_D}\dfrac{\partial}{\partial r_D}\left(r_D \dfrac{\partial \eta_{fD}^1}{\partial r_D}\right) \\ \quad = (1 - \Omega)\dfrac{1}{1 - \gamma_D \eta_{mD}^1}\dfrac{\partial \eta_{mD}^1}{\partial t_D} \\ \qquad + \Omega \dfrac{1}{1 - \gamma_D \eta_{fD}^1}\dfrac{\partial \eta_{fD}^1}{\partial t_D} \\ (1 - \Omega)\dfrac{1}{1 - \gamma_D \eta_{fD}^1}\dfrac{\partial \eta_{fD}^1}{\partial t_D} = -\Lambda_1(\eta_{mD}^1 - \eta_{fD}^1) \end{cases} \tag{22}$$

The inner boundary condition is

https://doi.org/10.1021/acsomega.3c04183
ACS Omega 2023, 8, 32892−32906

$$\begin{cases} C_D\left(\dfrac{1}{1-\gamma_D\eta_{wD}}\dfrac{\partial\eta_{wD}}{\partial t_D}-\dfrac{1}{1-\gamma_D\eta_{\varphi D}}\dfrac{\partial\eta_{\varphi D}}{\partial t_D}\right) \\ \quad -r_D e^{-\gamma p_{fD}^1}\dfrac{\partial\eta_{fD}^{(1)}}{\partial r_D}\Big|_{r_D=1} \\ \quad =1 \\ -\dfrac{1}{\gamma_D}\ln(1-\gamma_D\eta_{wD}) \\ \quad =\left(-\dfrac{1}{\gamma_D}\ln(1-\gamma_D\eta_{fD}^{(1)})-Sr_D\dfrac{\partial\eta_{fD}^{(1)}}{\partial r_D}\Big|_{r_D=1}\right) \end{cases} \tag{23}$$

The connection conditions in Zone-1 and Zone-2

$$-\frac{1}{\gamma_D}\ln(1-\gamma_D\eta_{fD}^{(1)}(R_{D1},t_D))=\eta_{fD}^{(2)}(R_{D1},t_D) \tag{24}$$

$$\frac{1}{1-\gamma_D\eta_{fD}^{(1)}}\frac{\partial\eta_{fD}^{(1)}}{\partial r_D}\Big|_{r_D=R_{D1}}=\frac{1}{M_2}\frac{\partial\eta_{fD}^{(2)}}{\partial r_D}\Big|_{r_D=R_{D1}} \tag{25}$$

According to the above equation, the equations for other interfaces can be obtained.

The approximate analytical solution can be obtained using the perturbation law. Because the dimensionless permeability modulus is usually small, η can be expanded as a power series in the parameter γ_D.[37,38]

$$\begin{cases} \eta_D=\eta_0+\gamma_D\eta_1+\gamma_D^2\eta_2+\cdots \\ \dfrac{1}{1-\gamma_D\eta}=1+\gamma_D\eta+\gamma_D^2\eta_2^2+\cdots \end{cases} \tag{26}$$

Submitting eq 26 into eqs 22, 22 can be expressed in the Laplace space as follows

$$\begin{cases} \dfrac{\partial^2\overline{\eta_{fD}^{(i)}}}{\partial r_D^2}+\dfrac{1}{r_D}\dfrac{\partial\overline{\eta_{fD}^{(i)}}}{\partial r_D}=(1-\Omega)u\,\overline{\eta_{mD}^{(i)}}+M_i\Omega u\,\overline{\eta_{fD}^{(i)}} \\ (1-\Omega)u\,\overline{\eta_{mD}^{(i)}}=-\Lambda_i(\overline{\eta_{mD}^{(i)}}-\overline{\eta_{fD}^{(i)}}) \end{cases} \tag{27}$$

where u is the Laplace transform variable. Equation 27 can be rewritten as

$$\frac{\partial^2\overline{\eta_{fD}^{(i)}}}{\partial r_D^2}+\frac{1}{r_D}\frac{\partial\overline{\eta_{fD}^{(i)}}}{\partial r_D}=M_i u f^i(u)\,\overline{\eta_{fD}^{(i)}} \tag{28}$$

where

$$f^{(i)}(u)=\frac{M_i[\Lambda_i+\Omega(1-\Omega)u]}{M_i\Omega(1-\Omega)+\Lambda_i} \tag{29}$$

In order to obtain the solution to eq 22, we model the saturation change by considering a sequence of N banks, as shown in Figure 3. Index j is used to refer to the banks, for which $j=1$ corresponds to the innermost bank around the well (oil and gas bank) and $j=N$ corresponds to the outermost bank (gas bank). The pressure and flux continuity in the interbank boundaries define the boundary conditions and relate the partial differential equations in each bank. The saturation is assumed to be constant in each bank.[39−41]

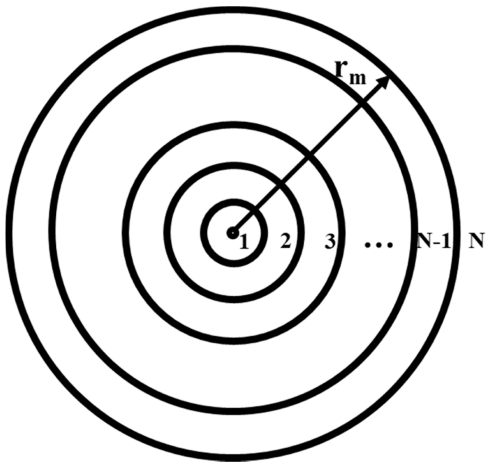

Figure 3. Schematic diagram of reservoir divided into N banks.

The general solution to eq 28 by Bessel function in Laplace space is[42]

$$\begin{cases} \overline{\eta}_{fD,j}^{(1)}=A_{1,j}K_0(r_D\cdot\sqrt{u\cdot f_j^{(1)}(u)})+B_{1,j}I_0(r_D\cdot\sqrt{u\cdot f_j^{(2)}(u)}) \\ \overline{\eta}_{fD,j}^{(2)}=A_{2,j}K_0(r_D\cdot\sqrt{u\cdot f_j^{(2)}(u)})+B_{2,j}I_0(r_D\cdot\sqrt{u\cdot f_j^{(2)}(u)}) \\ \overline{\eta}_{fD,j}^{(3)}=A_{3,j}K_0(r_D\cdot\sqrt{u\cdot f_j^{(3)}(u)})+B_{3,j}I_0(r_D\cdot\sqrt{u\cdot f_j^{(3)}(u)}) \\ \overline{\eta}_{fD,j}^{(4)}=A_{4,j}K_0(r_D\cdot\sqrt{u\cdot f_j^{(4)}(u)})+B_{3,j}I_0(r_D\cdot\sqrt{u\cdot f_j^{(4)}(u)}) \end{cases} \tag{30}$$

Note that in eq 30, the subscript j is added to various parameters to distinguish solutions for different banks. There are N sets of equations for N banks. Note also that, to calculate dimensionless parameters, the parameters of the first bank are taken ($j=1$) as reference.

Initially, for all regions j, the pressure in the matrix and the fractures are equal and constant.

$$\overline{\eta_{fD,j}^{i}}(r_D,0)=\overline{\eta_{mD,j}^{i}}(r_D,0)=0 \tag{31}$$

For the first bank ($j=1$), wellbore boundary conditions for flow and pressure, including wellbore storage and skin, are given as

$$\begin{cases} C_D u\,\overline{\eta_{wD}}-\dfrac{\partial\overline{\eta_{fD,1}^{1}}}{\partial r_D}\Big|_{r_D=1}=\dfrac{1}{u} \\ \overline{\eta_{wD}}=\left(\overline{\eta_{fD,1}^{1}}-S\dfrac{\partial\overline{\eta_{fD,1}^{1}}}{\partial r_D}\Big|_{r_D=1}\right) \end{cases} \tag{32}$$

The pressure and flux at the interface of each annular ring are continuous

$$\begin{cases} \overline{\eta_{fD,j}^{i}}=\overline{\eta_{fD,j+1}^{i}},\ @r_D=r_{D_j}^{i} \\ \dfrac{\partial\overline{\eta_{fD,j}^{i}}}{\partial r_D}=\dfrac{M_{i-1}}{M_i}\dfrac{\partial\overline{\eta_{fD,j+1}^{i}}}{\partial r_D},\ @r_D=r_{D_j}^{i},\ M_0=1 \end{cases} \tag{33}$$

The phase redistribution pressure is

https://doi.org/10.1021/acsomega.3c04183
ACS Omega 2023, 8, 32892−32906

$$\overline{\eta_{\varphi D}} = C_{\varphi D}\left(\frac{1}{u} - \frac{\alpha_D}{u\alpha_D + 1}\right) \tag{34}$$

For the outermost bank ($j = N$), the infinite boundary condition is given in eq 35, respectively.

$$\overline{\eta_{fD}^4}(\infty, u) = 0 \tag{35}$$

Through pressure boundary conditions, the coefficient B_N is 0.

$$\overline{\eta}_{fD,N}^4 = A_N K_0(r_D \cdot \sqrt{u \cdot f_j^4(u)}) \tag{36}$$

Hence, for each bank, a partial differential equation solution is given by eq 30 with two unknowns, A_j and B_j. Through the pressure and flux relationship at each interface, these equations can be related and solved for the coefficients A_j and B_j. The equations can be expressed in matrix form (eq 37)

$$\begin{bmatrix} a_{1,01} & a_{1,02} & 0 & \cdots & \cdots & \cdots & \cdots & 0 \\ a_{1,11} & a_{1,12} & a_{1,13} & a_{1,14} & 0 & \cdots & \cdots & 0 \\ b_{1,11} & b_{1,11} & b_{1,11} & b_{1,11} & 0 & \cdots & \cdots & 0 \\ 0 & 0 & a_{1,21} & a_{1,22} & a_{1,23} & a_{1,24} & \cdots & 0 \\ 0 & 0 & b_{1,21} & b_{1,22} & b_{1,23} & b_{1,24} & \cdots & 0 \\ \cdots & \cdots & \cdots & \cdots & \cdots & \cdots & \cdots & \cdots \\ 0 & \cdots & \cdots & \cdots & 0 & a_{4,N-1,1} & a_{4,N-1,2} & a_{4,N-1,3} \\ 0 & \cdots & \cdots & \cdots & 0 & b_{4,N-1,1} & b_{4,N-1,2} & b_{4,N-1,3} \end{bmatrix}$$

$$\begin{bmatrix} A_1 \\ B_1 \\ A_2 \\ B_2 \\ \cdots \\ A_{N-1} \\ B_{N-1} \\ A_N \end{bmatrix} = \begin{bmatrix} 1/u + C_D u \overline{p_{\varphi D}} \\ 0 \\ 0 \\ 0 \\ \cdots \\ 0 \\ 0 \\ 0 \end{bmatrix} \tag{37}$$

The elements of the matrix can be obtained by imposing boundary conditions. The first row in the matrix corresponds to the wellbore equations (eqs 38 and 39). Hence, a_{01} and a_{02} can be expressed as

$$a_{01} = C_D u[K_0(\sqrt{u \cdot f_1(u)}) + S\sqrt{u \cdot f_1^1(u)}\, K_1(\sqrt{u \cdot f_1^1(u)})] + \sqrt{u \cdot f_1^1(u)}\, K_1(\sqrt{u \cdot f_1^1(u)}) \tag{38}$$

$$a_{02} = C_D u[I_0(\sqrt{u \cdot f_1^1(u)}) - S\sqrt{u \cdot f_1^1(u)}\, I_1(\sqrt{u \cdot f_1^1(u)})] - \sqrt{u \cdot f_1^1(u)}\, I_1(\sqrt{u \cdot f_1^1(u)}) \tag{39}$$

The remaining row pairs with a and b terms describe the boundary conditions between adjacent banks as defined by eqs 40 and 41

$$\begin{cases} a_{i,j1} = K_0(r_{Dj}\sqrt{u \cdot f_j^i(u)}) \\ a_{i,j2} = I_0(r_{Dj}\sqrt{u \cdot f_j^i(u)}) \\ a_{i,j3} = -K_0(r_{Dj}\sqrt{u \cdot f_{j+1}^i(u)}) \\ a_{i,j4} = -I_0(r_{Dj}\sqrt{u \cdot f_{j+1}^i(u)}) \end{cases} \tag{40}$$

$$\begin{cases} b_{i,j1} = -M_i\sqrt{u \cdot f_j^i(u)}\, K_1(r_{Dj}\sqrt{u \cdot f_j^i(u)}) \\ b_{i,j2} = M_i\sqrt{u \cdot f_j^i(u)}\, I_1(r_{Dj}\sqrt{u \cdot f_j^i(u)}) \\ b_{i,j3} = M_{i-1}\sqrt{u \cdot f_{j+1}^i(u)}\, K_1(r_{Dj}\sqrt{u \cdot f_{j+1}^i(u)}) \\ b_{i,j4} = -M_{i-1}\sqrt{u \cdot f_{j+1}^i(u)}\, I_1(r_{Dj}\sqrt{u \cdot f_{j+1}^i(u)}) \end{cases} \tag{41}$$

Once the matrix is solved and the values of A_1 and B_1 are known, the Laplace domain solution can be obtained for the wellbore pressure

$$\overline{\eta_{wD}} = A_1[K_0(\sqrt{u \cdot f_1^1(u)}) + S\sqrt{u \cdot f_1^1(u)}\, K_1(\sqrt{u \cdot f_1^1(u)})] + B_1[I_0(\sqrt{u \cdot f_1^1(u)}) - S\sqrt{u \cdot f_1^1(u)}\, I_1(\sqrt{u \cdot f_1^1(u)})] \tag{42}$$

The solution p_{wD} can be found by converting the Laplace domain result in eq 42 to time domain by using the Stehfest algorithm.[43] The workflow of solution to plot the type curve is illustrated by the procedure depicted in Figure 4.

$$p_{wD} = -\frac{1}{\gamma_D}\ln(1 - \gamma_D \eta_{wD}) \tag{43}$$

3. VALIDATION AND LIMITATION

To verify the analytical model, a numerical simulation model is developed in a commercial simulator CMG compared with the semianalytical model using the same parameters. The properties of the reservoir and fluid are presented in detail in Table 2.

Figure 5 illustrates the constant volume depletion (CVD) test curve. Figure 6 shows the relative permeability relationships used in the model. Figure 7 displays a comparison between the results obtained from the commercial simulator and the proposed model. The excellent agreement between the proposed model and the commercial simulator demonstrates the reliability and accuracy of the proposed model.

4. RESULTS AND DISCUSSION

4.1. Type Curves. As shown in Figure 8, the type curve results are presented for two-phase flow considering the retrograde condensation, stress sensitivity, and wellbore phase redistribution. According to the BHP and its derivative curve, 10 flow regimes were determined.

Regime 1: Wellbore storage regime. The characteristic of the pressure and its derivative curves is a unit slope.**Regime 2**: The first transitional-flow regime. The derivative of dimensionless pressure will show a "gas hump" due to the influence of the skin effect and wellbore phase redistribution.**Regime 3**: Interporosity regime. The derivative curve shows a V-shape due to the flow from the matrix to the natural fractures.**Regime 4**: The first

https://doi.org/10.1021/acsomega.3c04183
ACS Omega 2023, 8, 32892−32906

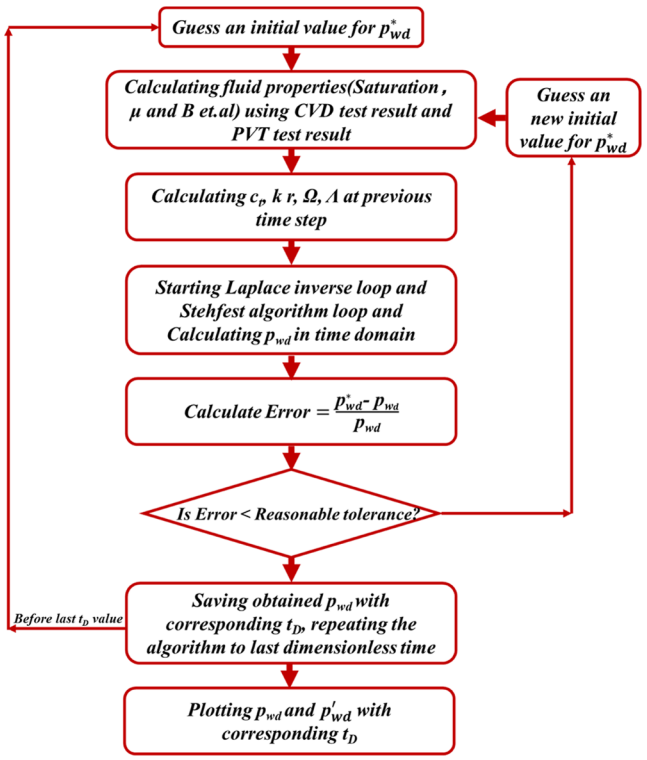

Figure 4. Procedure of solution for plotting PTA-type curves using the proposed method in this study.

Table 2. Gas Condensate Reservoir and Fluid Properties

parameters	value
porosity, %	5
temperature, K	445.05
reservoir thickness, m	50
original pressure, MPa	55
wellbore radius, m,	0.069
dew point pressure, MPa	40
maximum CVD liquid dropout, %	25.1
permeability, $10^{-3}\mu m^2$	2.5
rock compressibility, 1/MPa	1.45×10^{-6}

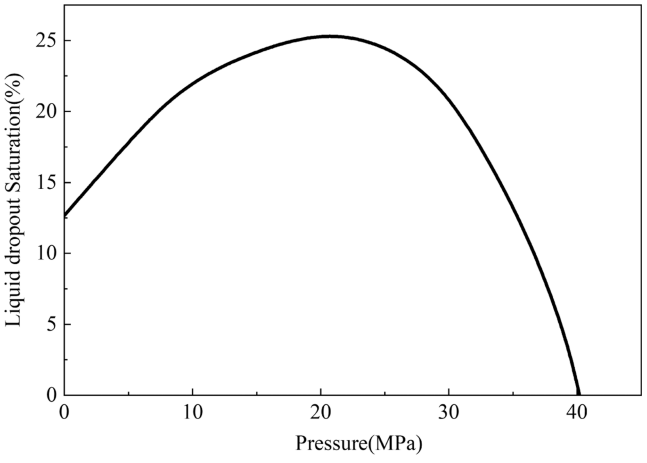

Figure 5. Plot of CVD liquid dropout curve.

radial flow regime, representing the oil-gas two-phase flow under the influence of capillary number. The pressure derivative curve is a horizontal line, whose value keeps at around 0.5.**Regime 5**: The second transitional-flow regime. The derivative curve shows an upward trend reflecting that the pressure wave spreads from Zone-1 to Zone-2.**Regime 6**: The second is the radial flow regime. The derivative curve transitions to a new horizontal line with a value of $0.5M_2$, representing the oil-gas two-phase flow independent of the capillary number.**Regime 7**: The third transitional-flow regime. The pressure derivative curve shows a downward trend, reflecting that the pressure wave spreads from Zone-2 to Zone-3.**Regime 8**: The third radial flow regime represents the flow of the gas phase in the condensate blockage area. It is represented by the pressure derivative horizontal line of $0.5*M_2*M_3$.**Regime 9**: The fourth transitional-flow regime. The pressure derivative curve continues to show a downward trend, reflecting that the pressure wave spreads from Zone-3 to Zone-4. The drop in the pressure derivative indicates a high fluidity in Zone-4.**Regime 10**: The fourth radial flow regime represents the gas flows radially toward the wellbore in Zone-4. It reflects the initial state of the condensate gas reservoir, where the horizontal line of the pressure derivative is $0.5*M_2*M_3*M_4$.In the regime of radial flow, the pressure derivative curve shows a trend of rising first and then declining, which suggests that mobility varies in different zones. However, depending on wellbore storage and well and reservoir dimensions, these flow regimes may appear, which is revealed in the sensitivity analysis.

4.2. Sensitivity Analysis. The BHP of FLPGCR is expected to be affected by the following factors, i.e., phase redistribution pressure parameter, permeability modulus, composite radius, storativity ratio, shape factor, and mobility ratio. The effects of the above parameters on BHP were investigated by using the FLPGCR model proposed in this paper.

4.2.1. Phase Redistribution Pressure Parameter $C_{\varphi D}$. The effects of different phase redistribution pressure parameters ($C_{\varphi D}$ = 0.5, 1, 2) on the transient pressure behavior are considered when other parameters are constant. Figure 9 shows the effects of the phase redistribution pressure parameter ($C_{\varphi D}$) on BHP and its derivatives. The "gas hump" is apparent when there are high values of $C_{\varphi D}$, while low values of $C_{\varphi D}$ lead to a significant reduction in the phase redistribution effect. The wellbore phase redistribution results in a two-segment distribution of the pressure derivative curve, both with slopes of 1. As the phase redistribution pressure parameter increases, more fluids are stored in the wellbore and the rate of pressure change slows down. Moreover, the duration of transition flow regimes increases as $C_{\varphi D}$ increases. In addition, with the increase in $C_{\varphi D}$, the first transition flow appears and ends later. However, it has no effect on the pressure behavior after the first transient flow regime.

4.2.2. Permeability Modulus γ_D. Figure 10 shows the dimensionless BHP behaviors when the permeability modulus is 0.01, 0.02, 0.05, 0.1, and 0.15. It can be clearly observed that the dimensionless BHP varies with the permeability modulus, except for the wellbore storage regime and the first transient flow regime. The pressure derivative curve appears upturned characteristic in the late regimes because of stress sensitivity. Throughout the testing process, there is a tendency for the dimensionless pressure and its derivative curve to rise as the permeability modulus increases. It is remarkable that the upturned characteristic of the pressure derivative curve at the late regime may also be caused by a closed boundary. Therefore, extra attention should be paid when the pressure derivative curve appears to be upwarped in the later regime it may be caused by stress sensitivity rather than a closed boundary.

https://doi.org/10.1021/acsomega.3c04183
ACS Omega 2023, 8, 32892−32906

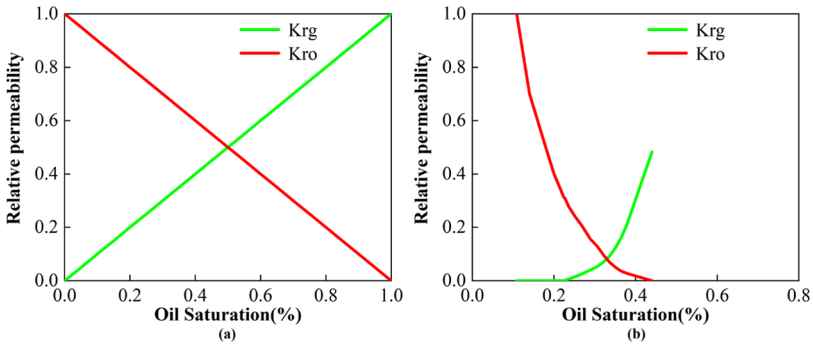

Figure 6. Relative permeability curve of fractures (a) and matrix (b)

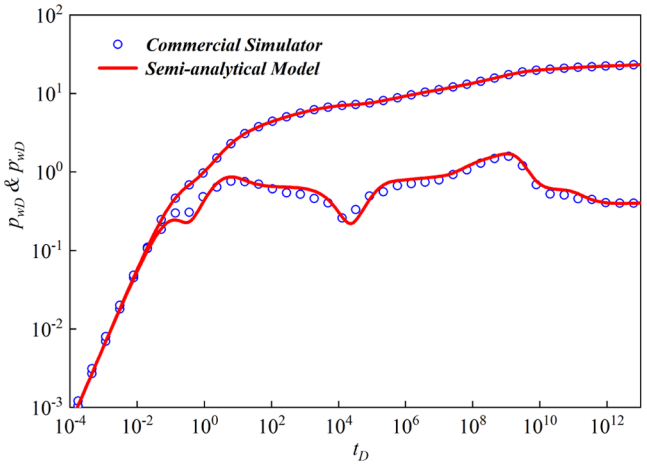

Figure 7. Results comparison between the commercial simulator and proposed model in this paper.

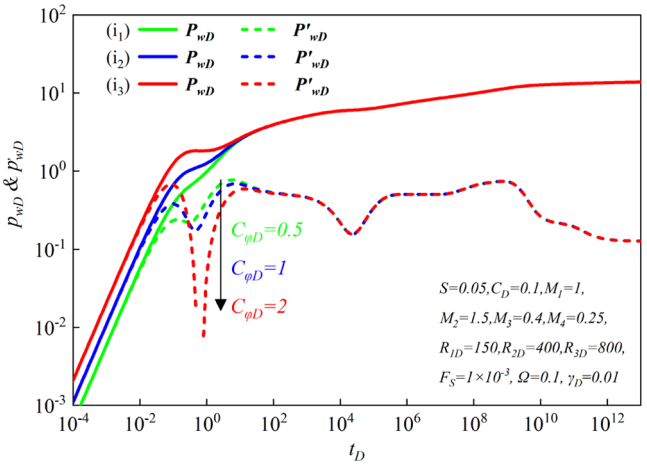

Figure 9. Effect of dimensionless phase redistribution pressure parameter ($C_{\varphi D}$) on type curves.

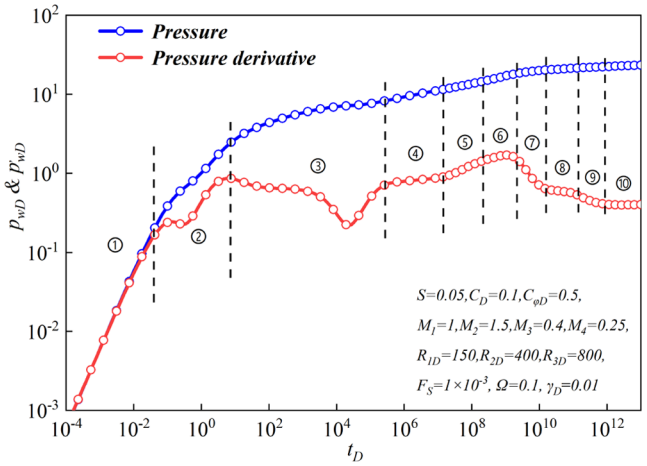

Figure 8. Type curve considering retrograde condensation, stress-sensitive, and wellbore phase redistribution.

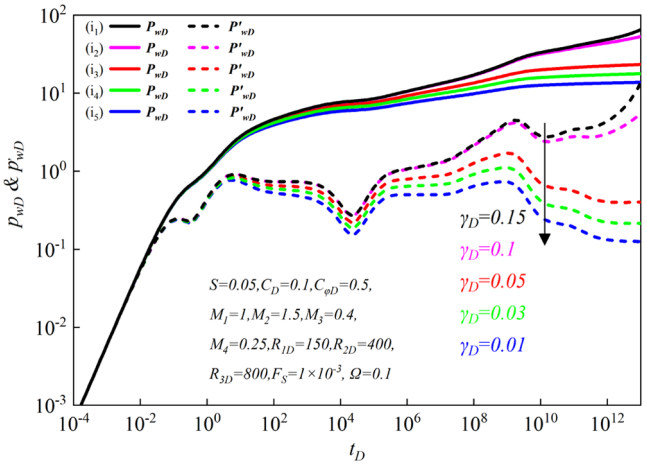

Figure 10. Effect of the permeability modulus (γ_D) on type curves

4.2.3. Composite Radius R_{jD}. Figure 11 shows the pressure and its derivative behaviors considering three cases of different composite radii (R_{1D}, R_{2D}, R_{3D}). R_{1D} is equal to 150, 200, and 300, respectively, while keeping R_{2D} and R_{3D} constant, and the results are shown in Figure 11a. As the value of Zone-1 radius increases, the duration of the first radial flow regime increases, whereas the characteristics of the second transition regime and the second radial flow regime are less obvious. The pressure derivative curves of other zones with the change of composite radius have the same trend as that of Zone-1. Therefore, it is possible to determine the range of the retrograde condensate region by analyzing the radial flow phase regime.

Furthermore, by summarizing the findings of Figure 11a–c, if the radius between two adjacent regions is similar, it is difficult for the four-zone feature to appear on the type curve. It tells us that even if retrograde condensation occurs in the formation, it may not be identified from the pressure test curve alone if the condensate bank is small. Therefore, sometimes it is necessary to determine the degree of condensate blockage by several pressure measurements.

https://doi.org/10.1021/acsomega.3c04183
ACS Omega 2023, 8, 32892−32906

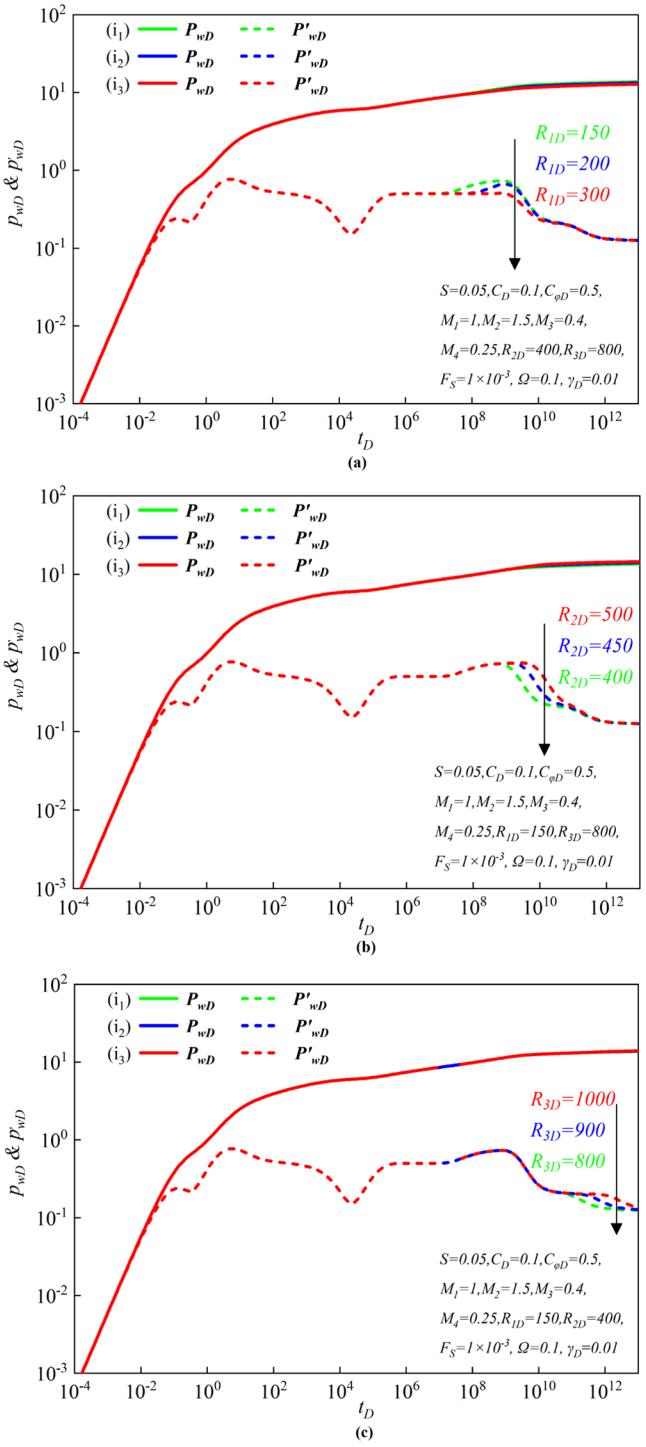

Figure 11. Effect of composite radius (R_{jD}) on type curves: (a) R_{1D}, (b) R_{2D}, (c) R_{3D}.

4.2.4. Shape Factor F_s. According to eq 13, two-phase interporosity flow coefficient Λ is a function of shape factor. Three cases of shape factor ($F_s = 1 \times 10^{-5}$, 1×10^{-4}, 1×10^{-3}) are selected in Figure 12a. The interporosity regime appears before the radial flow regime. The pressure and its derivative curves overlap except for the interporosity regime. The "V-shape" moves left as the shape factor. In other words, the larger the value of the shape factor, the earlier the "V-shape" appears. This is mainly because the shape factor mainly affects the interporosity regime. The larger shape factor makes it easier for

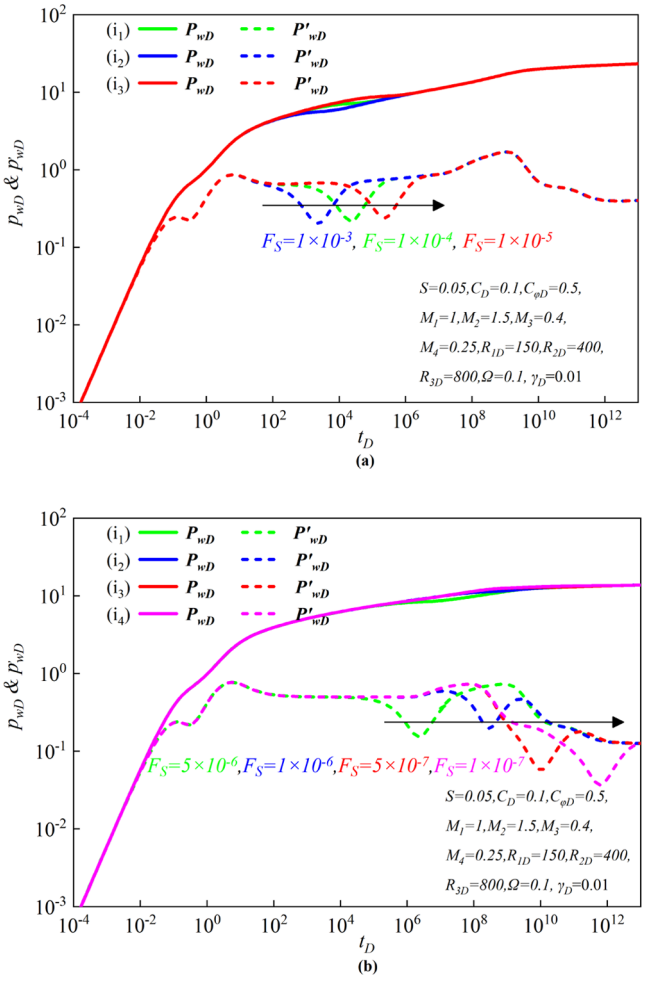

Figure 12. Effect of shape factor (F_s) on type curves: (a) F_s from 1×10^{-5} to 1×10^{-3}, (b) F_s from 1×10^{-7} to 5×10^{-6}.

fluid to flow between the matrix and the fracture, and the interporosity regime occurs earlier. It is worth noting that the "V-shape" appears in the position of the radial flow regimes as the value of shape factor decreases, which is shown in Figure 12b. For example, when the shape factor is equal to 1×10^{-7}, the V-shape appears in the position of Zone-2 and covers the characteristics of the second radial flow regime. This implies that the appearance of the interporosity regime is delayed with an increase in the degree of fracture development within the reservoir.

4.2.5. Two-phase Storativity Ratio Ω. The effect of the two-phase storativity ratio (Ω = 0.05, 0.1, 0.2) is analyzed, as shown in Figure 13. It can be seen from the results that except for the first transitional-flow regime and the interporosity regime, the pressure and its derivatives overlap in three cases. With the increases of Ω value, the storage ability of fracture decreases gradually. Meanwhile, the depth of the V-shape will become shallow and the start time of interporosity regime is delayed with the increase of Ω. This is because the fluid in the fracture flows out first when the formation pressure drops. That is, it takes a long time to produce an obvious pressure drop between the matrix and fracture if the fracture is large. The fluid in the matrix begins to flow toward the fracture until there is a significant pressure drop. Therefore, the more developed (which means a high number of fractures, large openings, and good con-

https://doi.org/10.1021/acsomega.3c04183
ACS Omega 2023, 8, 32892−32906

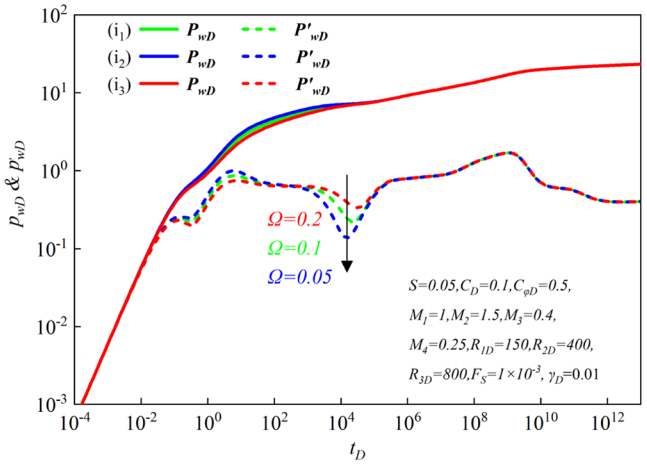

Figure 13. Effect of the two-phase stability ratio (Ω) on PTA-type curves.

nectivity) the fracture in the formation, the later the interporosity regime begins.

4.2.6. Different Mobility Ratio M_i. The effect of the mobility ratio is represented in Figure 14. The mobility ratio has little effect on the pressure curve and mainly affects the pressure derivative curve. Zone-2 (M_2) is taken as an example to analyze, as shown in Figure 14a. Three cases of Zone-2 mobility ratio M_2 (M_2 = 1.5, 2, and 2.5) are selected. It is evident that three cases of pressure and its derivative overlap except for the second transitional-flow regime and the second radial flow regime. It can be clearly noted that the pressure and its derivative curve rise after the first radial flow regime with the increase of M_2. Furthermore, the derivative curve of pressure shows that as M_2 decreases gradually, the characteristics of the second radial flow regime are covered, making the pressure transient response more similar to that of a three-zone system. The effect of the mobility ratio on the derivative curve is similar at different zones, as is shown in Figure 14b,c.

5. CASE STUDY

X Buried Hill gas condensate reservoir was discovered in recent years in China with a maximum liquid dropout of 15% at 22 MPa and a dew point pressure of 42.1 MPa. The seismic detection shows that fractures are developed in the reservoir. The experimental results demonstrate that the gas condensate reservoir exhibits low-permeability characteristics. A typical well in this field was interpreted to verify the practicability of the proposed model.

The basic parameters of the gas condensate reservoir and Well A are given in Table. 3. The test was conducted after the well had been in production for one year. Initially, the production was only gas. However, after a certain period, both oil and gas were produced simultaneously. Figure 15 shows the phase diagrams and fractured carbonated rock cores of Well A.

The commercial software KAPPA was used to interpret the pressure measurements obtained from well A. Figure 16 shows the interpretation results of the pressure measurements by using KAPPA's existing model. Among them, Figure 16a shows the interpretation result using the double-porosity model and Figure 16b shows the interpretation result using the radial composite model. It is evident that both models exhibit partial fitting only, resulting in an overall unsatisfactory level of fit.

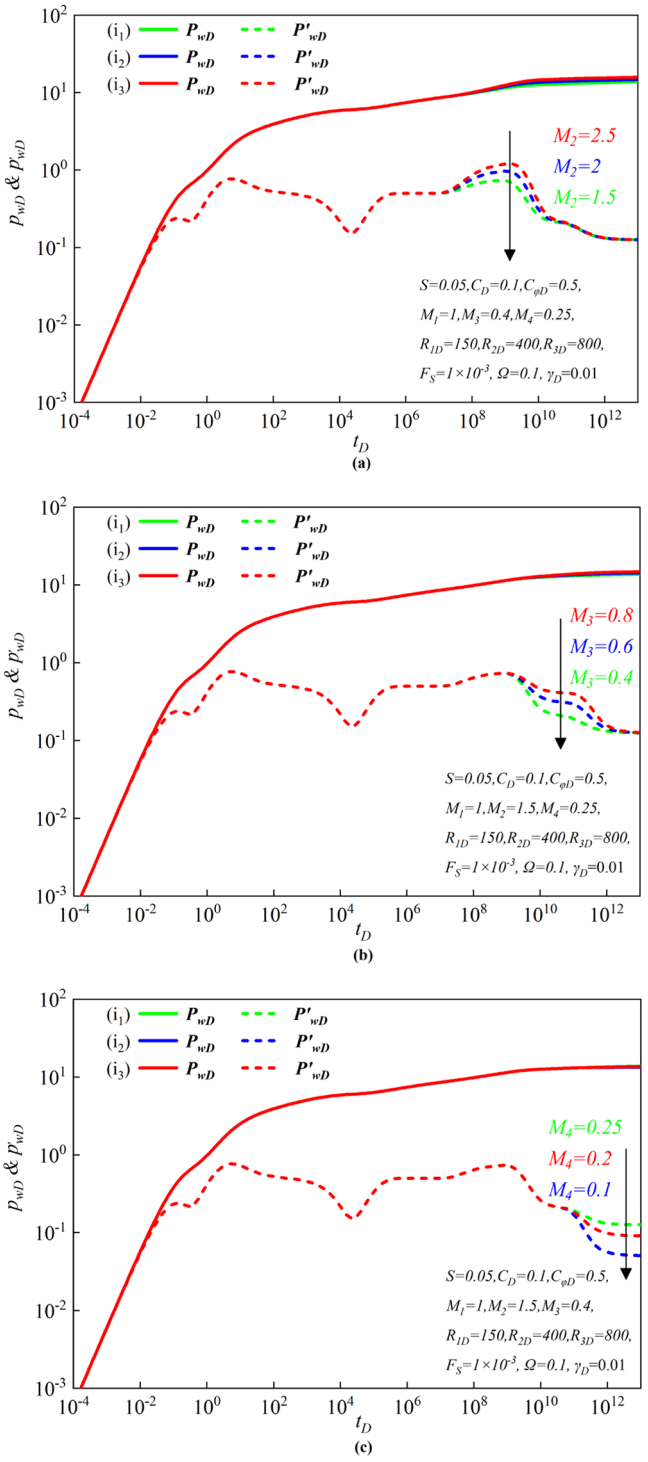

Figure 14. Effect of mobility ratio (M_i) on type curves: (a) M_2, (b) M_3, (c) M_4.

Next, the semianalytical model proposed in this paper was used to interpret the recorded pressure measurements. Figure 17 demonstrates a good fit between the recorded pressure measurements and the theoretical curve. The recorded transient pressure curve has the characteristics of fracture and matrix interporosity flow and also has the characteristics of multizone composite. Table. 4 shows the interpretation results. The proposed model offers a comprehensive understanding of various parameters, including the radius of each individual reverse condensate zone and the physical properties of the

https://doi.org/10.1021/acsomega.3c04183
ACS Omega 2023, 8, 32892−32906

Table 3. Basic Parameters of Reservoir and Well

parameters	value	sources
well depth, m	5499.8	well logging
temperature, K	445.05	well logging
original pressure, MPa	58.53	measurement
well radius, m	0.069	
porosity, %	5.43	experiment
permeability, 10^{-3} μm^2	2.5	experiment measurement
reservoir thickness, m	80	
dew point pressure, MPa	42.1	experiment
maximum CVD liquid dropout, %	15	experiment measurement

formation. Moreover, it facilitates a more precise depiction of the condensate distribution within the reservoir.

6. CONCLUSIONS

This work proposed a semianalytical model to investigate the pressure transient behavior of FLPGCR. We modeled the saturation profile as a multibank reservoir, in which the saturation and parameters associated with saturation are constant within each bank. We presented details of model development, validation, sensitivity analysis, and a case study. The proposed semianalytical model can be applied to interpret pressure measurements. The new model not only elucidates the fracture parameters but also provides a comprehensive characterization of the existing condensate oil distribution in the formation. This advancement will significantly enhance the efficiency of gas condensate reservoir development. Following are contributions and conclusions inferred from this study:

- A simple, fast, and stable semianalytical mathematical model is developed for a multiphase (oil and gas) well in FLPGCR. The derivation of the analytical approach is rigorously discussed, and the numerical simulation results are compared to results from the proposed model, which show excellent agreement in general.
- There are 10 flow regimes in our model, including the wellbore storage regime, the transitional-flow regime, interporosity regime, the first radial flow regime, the second transitional-flow regime, the second radial flow, the third transitional-flow regime, the third radial flow regime, the third transitional-flow regime, and the fourth radial flow regime.
- The wellbore phase redistribution has a significant influence in the early regime. Increasing the phase redistribution pressure parameter slows down pressure drop, prolongs transition flow regimes, and delays the

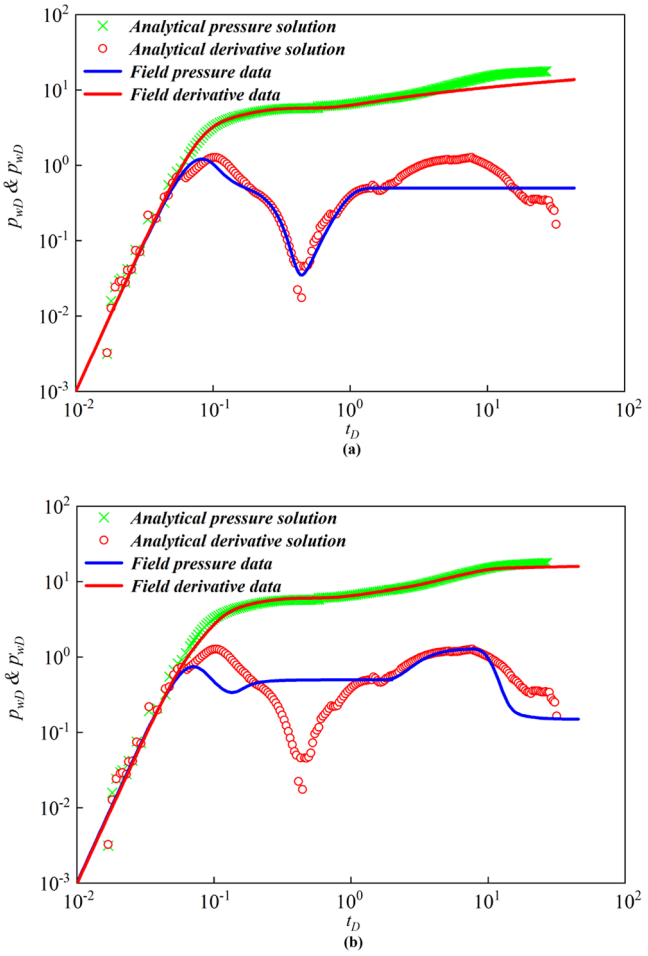

Figure 16. Analysis result of the commercial software KAPPA: (a) double-porosity model and (b) radial composite model.

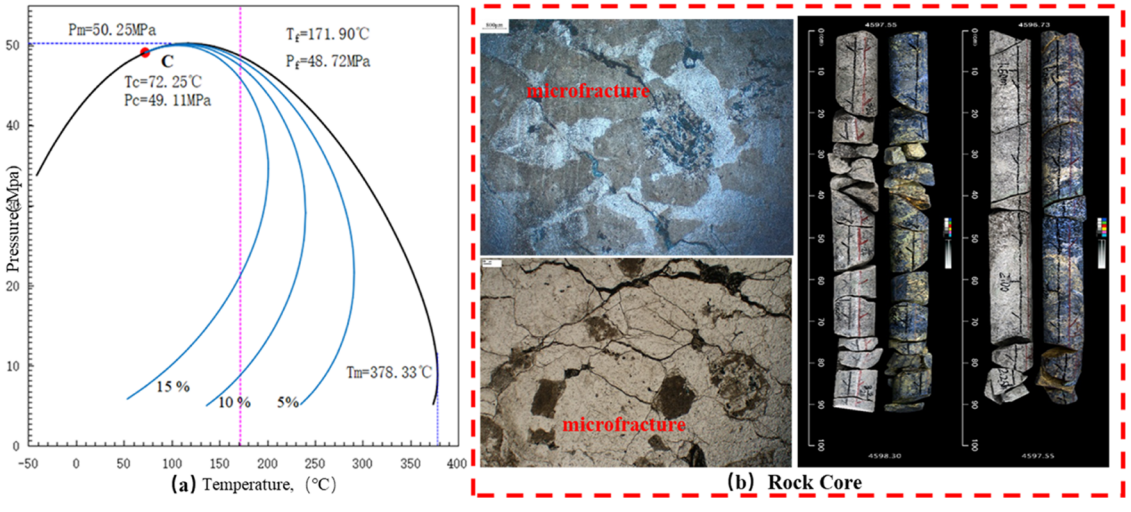

Figure 15. (a) Phase diagram and (b) the fracture characteristic exhibited in the rock core samples.

https://doi.org/10.1021/acsomega.3c04183
ACS Omega 2023, 8, 32892−32906

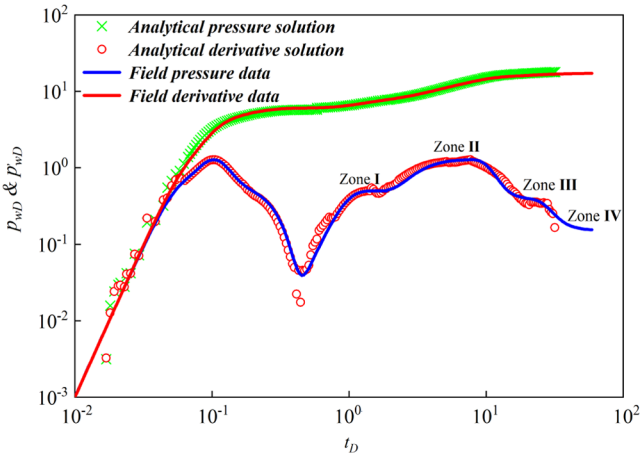

Figure 17. Application of the proposed semianalytical solution.

Table 4. Interpretations Results of Well A

parameters		symbol	unit	interpretation results
wellbore storage coefficient		C	m^3/MPa	0.98
skin factor		S		0.14
permeability	zone I	k_1	10^{-3} μm^2	1.07
	zone II	k_2		0.52
	zone III	k_3		1.52
	zone IV	k_4		2.31
composite radius	zone I	R_1	m	21.63
	zone II	R_2		61.26
	zone III	R_3		26.21
shape factor		F_s		2.1×10^{-5}
two-phase storativity ratio		Ω		0.23
permeability modulus		γ		0.01
phase redistribution pressure parameter		C_φ		0.2

onset and end of the first transition flow. The stress sensitivity could lead to the upturned characteristic of the curve in the late regime.

- The shape factor and composite radius may mask the radial flow regime. The shape factor mainly changes the position of the interporosity regime which may obscure the characteristics of the radius flow regime. In addition, if the radius of two adjacent zones is close, the radial flow characteristics of the latter zone may be obscured.

- A case study was conducted in the Bohai oil field, which indicates the proposed model can interpret the pressure measurements recorded from an FLPGCR. The proposed solution is feasible to analyze the radius of retrograde condensation and formation parameters.

APPENDIX—BASIC DIFFERENTIAL EQUATION OF FLOW IN DOUBLE-POROSITY RESERVOIR

Based on the mass conservation principle, the generalized form of the continuity equation for oil−gas flow can be written as

$$\text{fracture: } \frac{1}{r}\cdot\frac{\partial(r\rho_i v_i)}{\partial r} + \frac{\partial\left(\frac{\varphi_f S_i}{B_i}\rho_i\right)}{\partial t} - q_m = 0,\ i = o, g$$

$$\text{matrix: } \frac{\partial\left(\frac{\varphi_f S_i}{B_i}\rho_i\right)}{\partial t} + q_m = 0 \tag{A-1}$$

q_m refers to the mass of fluid flowing from the matrix to the fracture per unit time.

$$q_m = F_s\rho_i\frac{K_m K_{mri}}{\mu_i B_i}(p_m - p_f),\ i = o, g \tag{A-2}$$

The permeability of fracture is obtained by integrating eq 1

$$K_f/K = e^{-\gamma(p_i - p)} \tag{A-3}$$

The equation of motion can be expressed as follows

$$v_o = -Ke^{-\gamma(p_i-p)}\frac{K_{rfo}}{\mu_o B_o}\frac{\partial p}{\partial r}$$

$$v_g = -Ke^{-\gamma(p_i-p)}\left(\frac{K_{rfg}}{\mu_g B_g} + \frac{R_s K_{rfo}}{\mu_o B_o}\right)\frac{\partial p}{\partial r} \tag{A-4}$$

The state equation can be expressed as follows

$$\varphi_j = \varphi_{j0}[1 + C_{j\varphi}(p - p_0)],\ j = m, f$$

$$\rho_i = \rho_{i0}[1 + C_{i\rho}(p - p_0)],\ i = o, g \tag{A-5}$$

Substituting eqs A-2−A-4 into eq A-1, the flow equation in fracture can be expressed as follows

$$\frac{1}{r}\frac{\partial}{\partial r}\left[r\left(\frac{K_{1f}e^{-\gamma(p_i-p)}K_{rfo}}{\mu_o B_o}\right)\frac{\partial p}{\partial r}\right] = F_s\frac{K_{1m}K_{rmo}}{\mu_o B_o}(p_m - p_f) + S_{fo}\phi_f c_{fto}\frac{\partial p_f}{\partial t} \tag{A-6}$$

$$\frac{1}{r}\frac{\partial}{\partial r}\left[rK_{1f}e^{-\gamma(p_i-p)}\left(\frac{K_{rfg}}{\mu_g B_g} + \frac{K_{rfo}}{\mu_o B_o}R_s\right)\frac{\partial p}{\partial r}\right] = F_s\left(\frac{K_{1m}K_{rmg}}{\mu_g B_g} + \frac{K_{1m}K_{rmo}}{\mu_o B_o}R_s\right)(p_m - p_f) + S_{fg}\phi_f c_{ftg}\frac{\partial p_f}{\partial t} \tag{A-7}$$

The flow equation in matrix can be expressed as follows

$$F_s\frac{K_{1m}K_{1mro}}{\mu_o}(p_m - p_f) + S_{mo}\phi_m c_{mto}\frac{\partial p_m}{\partial t} = 0 \tag{A-8}$$

$$F_s\left(\frac{K_{1m}K_{mrg}}{\mu_g} + \frac{K_{1m}K_{mro}}{\mu_o}R_s\right)(p_m - p_f) + S_{mg}\phi_m c_{mtg}\frac{\partial p_m}{\partial t} = 0 \tag{A-9}$$

where total compressibility coefficient c_{itj} can be expressed as follows

https://doi.org/10.1021/acsomega.3c04183
ACS Omega 2023, 8, 32892−32906

$$c_{fto} = c_f + c_o$$
$$c_{ftg} = c_f + c_g$$
$$c_{mto} = c_m + c_o$$
$$c_{mtg} = c_m + c_g \quad \text{(A-10)}$$

The two-phase total compressibility coefficient c_{jt} can be expressed as follows

$$c_{ft} = S_{fo}c_{fto} + S_{fg}c_{ftg}$$
$$c_{mt} = S_{mo}c_{mto} + S_{mg}c_{mtg} \quad \text{(A-11)}$$

The mobility can be expressed as

$$m_f = K_f\left(\frac{K_{rfo}}{\mu_o B_o} + \frac{K_{rfg}}{\mu_g B_g} + \frac{K_{rfo}}{\mu_o B_o}R_s\right)$$
$$m_m = K_m\left(\frac{K_{rmo}}{\mu_o B_o} + \frac{K_{rmg}}{\mu_g B_g} + \frac{K_{rmo}}{\mu_o B_o}R_s\right) \quad \text{(A-12)}$$

Substituting eqs A-11 and A-12 into eqs A-6−A-9, the total flow equation of Zone-1 between fracture and matrix can be expressed as

$$m_f\frac{1}{r}\frac{\partial}{\partial r}\left[re^{-\gamma(p_i-p)}\frac{\partial p}{\partial r}\right] = m_m F_s(p_m - p_f) + \phi_f c_{ft}\frac{\partial p_f}{\partial t} \quad \text{(A-13)}$$

$$F_s m_m(p_m - p_f) + \phi_m c_{mt}\frac{\partial p_m}{\partial t} = 0 \quad \text{(A-14)}$$

AUTHOR INFORMATION

Corresponding Author

Fuguo Yin − *State Key Laboratory of Petroleum Resources and Engineering, China University of Petroleum, Beijing, Beijing 102249, China;* orcid.org/0009-0005-4646-741X; Email: cupb65265764@163.com

Authors

Shiqing Cheng − *State Key Laboratory of Petroleum Resources and Engineering, China University of Petroleum, Beijing, Beijing 102249, China;* orcid.org/0000-0001-5267-5569

Xiuwei Liu − *State Key Laboratory of Petroleum Resources and Engineering, China University of Petroleum, Beijing, Beijing 102249, China*

Lijun Zhang − *Beijing Research Center of China National Offshore Oil Corporation, Beijing 100027, China*

Huisheng Liu − *China Oilfield Services Limited, Tianjin 300459, China*

Wenpeng Bai − *State Key Laboratory of Petroleum Resources and Engineering, China University of Petroleum, Beijing, Beijing 102249, China*

DengKe Shi − *State Key Laboratory of Petroleum Resources and Engineering, China University of Petroleum, Beijing, Beijing 102249, China*

Yang Wang − *State Key Laboratory of Petroleum Resources and Engineering, China University of Petroleum, Beijing, Beijing 102249, China*

Complete contact information is available at: https://pubs.acs.org/10.1021/acsomega.3c04183

Notes

The authors declare no competing financial interest.

ACKNOWLEDGMENTS

The authors thank the editors and reviewers for their valuable suggestions and important contributions to the improvement of this manuscript. They acknowledge the financial support from the Strategic Cooperation Technology Projects of CNOOC and CUPB (CCL2021RCPS0298RSN).

NOMENCLATURE

γ =permeability modulus, mPa·s/MPa^2
γ_D =dimensionless permeability modulus
K_{1f} =Zone I permeability in the fractures, 10^{-3} μm^2
K_{1m} =Zone I permeability in the matrix, 10^{-3} μm^2
k_{rfg} =relative permeability of gas in the fractures, 10^{-3} μm^2
k_{rmg} =relative permeability of gas in the matrix, 10^{-3} μm^2
k_{rfo} =relative permeability of oil in the fractures, 10^{-3} μm^2
k_{rmo} =relative permeability of oil in the matrix, 10^{-3} μm^2
ϕ_m =matrix system porosity, %
ϕ_f =fracture system porosity, %
μ_g =gas viscosity, mPa·s
μ_o =oil viscosity, mPa·s
S_{fo} =oil saturation in the fractures, %
S_{fg} =gas saturation in the fractures, %
S_{mo} =oil saturation in the matrix, %
S_{mg} =gas saturation in the matrix, %
c_{fto} =oil compressibility in the fractures, MPa^{-1}
c_{mto} =oil compressibility in the matrix, MPa^{-1}
c_{ftg} =gas compressibility in the fractures, MPa^{-1}
c_{mtg} =gas compressibility in the matrix, MPa^{-1}
c_{ft} =total compressibility in the fractures, MPa^{-1}
c_{mt} =total compressibility in the matrix, MPa^{-1}
c_o =oil compressibility, MPa^{-1}
c_g =gas compressibility, MPa^{-1}
B_o =oil volume factor
B_g =gas volume factor
p_m =pressure in the matrix, MPa
p_{Dm} =dimensionless matrix pressure
p_f =pressure in the fracture, MPa
p_{Df} =dimensionless fracture pressure
pi =initial reservoir pressure, MPa
C =wellbore storage coefficient, m^3/MPa
C_D =dimensionless wellbore storage coefficient
$C_{\varphi D}$ =dimensionless phase redistribution pressure parameter
R_s =Dissolved gas−oil ratio, m^3/m^3
F_s =shape factor
t =time, h
t_D =dimensionless time
r_w =wellbore radius, m
r =radial distance, m
r_D =dimensionless radial distance
S =skin factor
Λ =two-phase interporosity flow coefficient interporosity flow coefficient
Ω =two-phase storativity storativity
M_{if} =Zone i mobility in the fractures
M_{1m} =Zone i mobility in the matrix
α_D =dimensionless phase redistribution time parameter
η =Pedrosa variable
A,B =coefficient of Bessel function

https://doi.org/10.1021/acsomega.3c04183
ACS Omega 2023, 8, 32892−32906

SPECIAL FUNCTIONS

$I_0(x)$=Bessel function of the first kind
$K_0(x)$=Bessel function of the second kind

SUBSCRIPTS

i =Zone i
j =index referring to banks
D =dimensionless
f =fracture system
m =matrix system
u =Laplace variable
— =Laplace space

REFERENCES

(1) Roussennac, B. Gas Condensate Well Test Analysis, M.S. Thesis, Stanford University, 2001.
(2) Gondouin, M.; Iffly, R.; Husson, J. An Attempt to Predict the Time Dependence of Well deliverability in Gas-Condensate Fields. *SPE J.* **1967**, *7*, 113−124.
(3) Yu, X.; Lei, S.; Liangtian, S.; Shilun, L. In *A New Method for Predicting the Law of Unsteady Flow Through,Porous Medium on Gas Condensate Well*, Paper SPE35649 Presented at SPE Program Conference, Canada, April 28−May 1, 1996.
(4) Bloom, S. M. P.; Hagoort, J. In *The Combine Effect of Near-Critical Relative Permeability and Non-Darcy Flow on Well Impairment by Condensate Drop-Out*, Paper SPE 39976 Presented at the 1998 SPE Gas Technology Symposium, Canada, March 15−18, 1998.
(5) Kniazeff, V. J.; Nvaille, S. A. Two-phase flow of volatile hydrocarbons. *SPE J.* **1965**, *5* (37), 234−235.
(6) Luis, F. A.; Turgay, E.; Michael, A. Numerical analysis of multi-mechanistic flow effects in naturally fractured gas-condensate systems. *J. Pet. Sci. Eng.* **2007**, *58*, 13−29.
(7) Zhou, C.; Wu, X.; Li, H.; et al. Optimization of methods for liquid loading prediction in deep condensate gas wells. *J. Pet. Sci. Eng.* **2016**, *146*, 71−80.
(8) Muskat, M. *Physical Principles of Oil Production*; McGraw-Hill Book Company, Inc., 1949.
(9) O'Dell; Miller. Successfully Cycling a Low Permeability High-Yield Gas-Condensate Reservoir. *J. Pet.Technol.* **1967**, 41−47.
(10) Jones, J. R.; Raghavan, R. In *Interpretation of Flowing Well Responsein Gas Condensate Wells*, Paper SPE 14204 Presented at the1985 SPE Annual Technical Conference and Exhibition, Las Ve-gas, Sept 22−25.
(11) Jones, J. R.; Raghavan, R. Interpretation of Pressure Buildup Reservoirsin Gas Condensate Well. *SPEFE* **1989**, 93−104.
(12) Fevang, Ø.; Whitson, C. H. Modeling gas-condensate well deliver-ability. *SPE Res. Eng.* **1996**, *11* (4), 221−230, DOI: 10.2118/30714-PA.
(13) Xu, S.; Lee, J. W. In *Two-phase Well Test Analysis of Gas Condensate Reservoirs*, SPE Annual Technical Conference and Exhibition, Society of Petroleum Engineers: Houston, TX, 1999.
(14) Gringarten, A. C.; AAI-Lamki, S.; Daungkaewet.; et al. Well test analysis in gas-condensate reservoirs. *SPE* **2000**, 62920.
(15) Barrios, K.; Stewart, G.; Davies, D. A Novel Methodology for the Analysis of Well Test Responses in Gas Condensate Reservoirs. *Society of Petroleum Engineers*, 2003.
(16) Abdolnabi, H.; Nicolas, L.; Gringarten, A. In *Well Test Analysis of Horizontal Wells in Gas-Condensate Reservoirs*, SPE Annual Technical Conference and Exhibition, 2004.
(17) Gringarten, A.; Bozorgzadeh, M.; Hashemi, A.et al. In *Well Test Analysis in Lean Gas Condensate Reservoirs: Theory and Practice*, SPE Russian Oil and Gas Technical Conference and Exhibition, 2006.
(18) Bozorgzadeh, M.; Gringarten, A. C. In *New Estimate for the Radius of a Condensate Bank from Well Test Data Using Dry Gas PseudoPressure*, Paper SPE 89904, Presented at the SPE Technical Conference and Exhibition held in Houston, Texas, U.S.A., Sept 26−29, 2004.
(19) Kgogo, T. C.; Gringarten, A. C. In *Comparative Well-Test Behaviours in Low-Permeability Lean, Medium-Rich and Rich Gas Condensate Reservoirs*, SPE Paper 134452 Presented at the Annual Technical Conference and Exhibition, Florence, Italy, Sept 19−22, 2010.
(20) Aluko, A. O.; Gringarten, A. C. In *Well Test Dynamics of Rich Gas Condensate Reservoirs under Gas Injection*, SPE 121848, Paper Submitted for Presentation at the SPE EUROPEC 2009 Seminar Held in the Amsterdam, The Netherlands, June 8−11, 2009.
(21) Shahbazi, S.; Maarefvand, P.; Gerami, S. Transient pressure test analysis of horizontal wells in gas condensate reservoirs: Evaluation of conventional multi-phase pseudo-pressure solutions. *J. Pet. Sci. Eng.* **2016**, *145*, 668−688.
(22) Zhang, W.; Cui, Y.; Jiang, R.; et al. Production performance analysis for horizontal wells in gas condensate reservoir using three-region model. *J. Nat. Gas Sci. Eng.* **2019**, *61*, 226−236.
(23) Li, J.; Zhao, G.; Jia, X.; et al. Integrated study of gas condensate reservoir characterization through pressure transient analysis. *J. Nat. Gas Sci. Eng.* **2017**, *46*, 160−171.
(24) Dastan, A.; Kamal, M. M.; Hwang, Y.et al. In *Falloff Testing Under Multiphase Flow Conditions in Naturally Fractured Reservoirs*, SPE Western Regional Meeting, 2018.
(25) Dahim, S.; Taghavinejad, A.; Razghandi, M.; et al. Pressure and rate transient modeling of multi fractured horizontal wells in shale gas condensate reservoirs. *J. Pet. Sci. Eng.* **2020**, *185*, No. 106566.
(26) Warren, J. E.; Root, P. J. The behaviorofnaturally fractured reservoirs. *Soc. Pet. Eng. J.* **1963**, *3*, 245−255.
(27) Aguilera, R. Well test analysis of dual-porosity systems intercepted by hydraulic vertical fractures of finite conductivity. *SPE* **1989**, No. 18948, DOI: 10.2118/18948-MS.
(28) Wang, Y.; Yang, W.; Cheng, S.; Shiqing, C.; Zhang, K.; Kaidi, Z. Investigation on the Transient Pressure Response of Water Injector Coupling the Dynamic Flow Behaviors in the Wellbore, Waterflood-Induced Fracture and Reservoir: Semi-Analytical Modeling and A Field Case. *Int. J. Heat Mass Transfer* **2019**, *130*, 668−679.
(29) Yang, W.; Shiqing, C.; Jiazheng, Q.; et al. Development Theory and Practice of Water Injection Induced Fractures in Ultra-Low Permeability Reservoirs (in Chinese). *Sci. Sin. Technol.* **2022**, *52*, 613−626.
(30) Wei, C.; Liu, Y.; Deng, Y.; Cheng, S.; Hassanzadeh, H. Temperature Transient Analysis of Naturally Fractured Geothermal Reservoirs. *SPE J.* **2022**, *27*, 2723−2745.
(31) Computer Modeling Group (CMG). *IMEX User Manual, MYR2017 Version*, Calgary, Alberta, Canada, 2017.
(32) Saleh, A. M.; Stewart, G. Interpretation of Gas Condensate Well Tests With Field Examples. *SPE* **1992**, No. 24719, DOI: 10.2118/24719-MS.
(33) Duangkaew, S.; Ross, F.; Gringarten, A. C. In *Well Test Analysis of Condensate Drop-out Behavior in a North Sea Len Gas Condensate Reservoir*, Paper SPE-77548 Presented at the SPE Annual Technical Conference and Exhibition, San Antonio, Texas, Sept 29−Oct 2, 2002.
(34) Rangel-German, E. R.; Kovscek, A. R. Matrix-Fracture Shape Factors and Multiphase-Flow Properties of Fractured Porous Media, *Society of Petroleum Engineers*, 2005.
(35) Fair, W. B. Pressure Buildup Analysis With Wellbore Phase Redistribution. *SPE J.* **1981**, *21*, 259−270.
(36) Pedrosa, O. A. In *Pressure Transient Response in Stress-Sensitive Formations*. Paper presented at the SPE California Regional Meeting, Oakland, California, April 1986.
(37) Kikani, J.; Oswaldo, A. P. Perturbation Analysis of Stress-Sensitive Reservoirs. *SPE Form. Eval.* **1991**, *6*, 379 DOI: 10.2118/20053-PA.
(38) Guo, J.; Wang, H.; Zhang, L.; et al. Pressure transient Analysis and flux distribution for Multistage fractured horizontal wells in triple-porosity reservoir media with consideration of stress-sensitivity effect. *J. Chem.* **2015**, *2015*, No. 212901, DOI: 10.1155/2015/212901.
(39) Abbaszadeh, M.; Kamal, M. Pressure-Transient Testing of Water-Injection Wells. *SPE Res. Eng.* **1989**, *4* (1), 115−124. SPE-16744-PA

https://doi.org/10.1021/acsomega.3c04183
ACS Omega 2023, 8, 32892−32906

(40) Bratvold, R. B. An Analytical Study of Reservoir Pressure Response Following Cold Water Injection, PhD dissertation, Stanford University: Stanford, CA, 1989.
(41) Nanba, T.; Horne, R. N. In *Estimation of Water and Oil Relative Permeabilities From Pressure Transient Analysis of Water Injection Well Data*, Paper SPE 19829 Presented at the 64th Annual Technical Conference and Exhibition of the Society of Petroleum Engineers, San Antonio, Texas, Oct 8−11, 1989.
(42) Kong, X. Y. *Advanced Mechanics of Fluids in Porous Media*, 2nd ed.; University of Science and Technology of China Press, 2010.
(43) Stehfest, H. Algorithm 368: Numerical inversion of Laplace transforms. *Commun. ACM* **1970**, *13* (1), 47−49.

https://doi.org/10.1021/acsomega.3c04183
ACS Omega 2023, 8, 32892−32906